Mechanical responses of submarine power cables subject to axisymmetric loadings

Fang, Pan; Jiang, Xiaoli; Hopman, Hans; Bai, Yong

DOI
10.1016/j.oceaneng.2021.109847

Publication date
2021

Document Version
Final published version

Published in
Ocean Engineering

Citation (APA)
Fang, P., Jiang, X., Hopman, H., & Bai, Y. (2021). Mechanical responses of submarine power cables subject to axisymmetric loadings. *Ocean Engineering*, *239*, Article 109847. https://doi.org/10.1016/j.oceaneng.2021.109847

Ocean Engineering 239 (2021) 109847

Contents lists available at ScienceDirect

Ocean Engineering

journal homepage: www.elsevier.com/locate/oceaneng

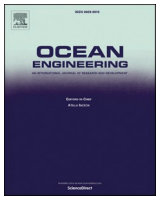

Mechanical responses of submarine power cables subject to axisymmetric loadings

Pan Fang [a,*], Xiaoli Jiang [a], Hans Hopman [a], Yong Bai [b]

[a] Department of Maritime and Transport Technology, Delft University of Technology, Netherlands
[b] College of Civil Engineering and Architecture, Zhejiang University, Hangzhou, Zhejiang, PR China

ARTICLE INFO

Keywords:
Submarine power cables
Axisymmetric loadings
Analytical method
Finite element method

ABSTRACT

Submarine power cables are considered lifelines in wind farm engineering, playing a key role in transporting electric current produced by wind turbines or wave converter. Cables inevitably confront combined loadings in deep-sea areas, affecting the integrity and safety during their installation and application. In this paper, the mechanical behaviour of submarine power cables subject to axisymmetric loadings(tension, torsion and external pressure) is investigated through both analytical and numerical methods. The objective of the analytical method is to predict the tension and torsion stiffness of cables and evaluate the stress of armour wires. These values from the two methods are essentially in agreement with each other. In addition, the effects of wire layers, winding angles and external pressure are discussed through the analytical method. The obtained conclusions will benefit the cross-section design of power cables and relative practical engineering.

Authorship statement

Manuscript title: Mechanical Responses of Submarine Power Cables Subject to Axisymmetric loadings.

All persons who meet authorship criteria are listed as authors, and all authors certify that they have participated sufficiently in the work to take public responsibility for the content, including participation in the concept, design, analysis, writing, or revision of the manuscript. Furthermore, each author certifies that this material or similar material has not been and will not be submitted to or published in any other publication before its appearance in the *Journal of Ocean Engineering*.

Authorship contributions

Please indicate the specific contributions made by each author. The name of each author must appear at least once in each of the three categories below.

Category 1.

Conception and design of study: Pan Fang, Xiaoli Jiang

Acquisition of data: Pan Fang

Analysis and/or interpretation of data: Pan Fang

Category 2.

Drafting the manuscript: Pan Fang

Revising the manuscript critically for important intellectual content: Pan Fang, Xiaoli Jiang

Category 3.

Approval of the version of the manuscript to be published (the names of all authors must be listed):

Xiaoli Jiang, Hans Hopman, Yong Bai,

1. Introduction

As the thirst for clean energy is growing hugely, the past few decades have witnessed an increase in wind farms, especially those built in deeper and more distant oceans where more abundant wind energy could be converted to electricity. Power cables are a vital and indispensable component in wind farm engineering since it plays a significant role in transporting the electricity. In order to ensure that it works safely and reliably during its serving time, the mechanical properties of cables must be carefully studied before it heads into the ocean. However, this structure's mechanical behaviour is not easily attainable because power cables are a type of extremely complex structure, composed of many layers and different materials. Each cable has a specific design based on its own purpose. Nevertheless, typical power cables are majorly composed of conductor, insulation, armour and serving. Fig. 1 gives, for example, a single core and three core cable.

* Corresponding author.
E-mail address: P.Fang-1@tudelft.nl (P. Fang).

https://doi.org/10.1016/j.oceaneng.2021.109847
Received 6 May 2021; Received in revised form 20 August 2021; Accepted 11 September 2021
Available online 20 September 2021

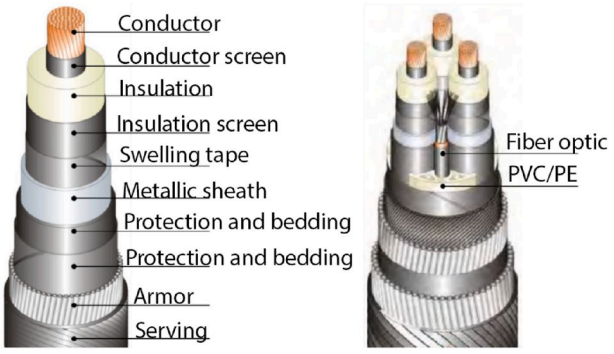

Fig. 1. Typical configuration of power cables.

There is a vast amount of research related to the mechanical study of structures like power cables, such as the study of flexible pipes or umbilicals. The similarities of these flexible structures lie in that they are all composed of many layers with different materials. However, helical wires, shown in Figs. 2 and 3, is one of the most used components in the flexible structures as it is capable of supporting high axial loads with comparatively high flexibility. In fibre glass reinforced flexible pipes (Fang et al., 2018; Xu et al., 2019), the hair-like fibres embedded in the polyethylene matrix is helical structure; In the umbilicals and cables (Sævik, 2010; Skeie et al., 2012), the tensile armour wire, usually made of steel with a rectangular or circular cross section, is helical structure; So is the metallic steel strip inside metallic strip flexible pipes (Fang et al., 2019; Bai et al., 2016a).

The study of helical structure could date back to Costello and Phillips (1974), where the wires were first used in bare wire cables that are not surrounded by outer layers. The theory used and developed in the early studies usually involves many assumptions and simplifications such as ignoring the interaction between adjacent layers. Knapp (1975) derived a new stiffness matrix for helically armoured cables considering tension and torsion based on the energy method. According to Knapp (1975), the resultant force and moment acting on the helix cross sections are obtained by taking into account the geometry and deformation of helical wires. Considering six nonlinear differential equations that describe the equilibrium of thin rods, Costello and Phillips (1975) treat the cables as groups of separate curved rods, giving a rigorous derivation based on Love (2013). Feret and Bournazel (Feret and Bournazel, 1987)proposed a simplified formulation to calculate the stress and contact pressure among different layers under axisymmetric loads. Many scholars, such as Ramos Jr and Kawano (Ramos and Kawano, 2015) and (Witz and Tan, 1992), divide the structure types inside cables, flexible pipes and umbilicals into two essential components: cylindrical elements and helical elements. The holistic behaviour of a flexible structure is dealt with as the combination of those two types of components considering the contact issue between each layer. Unlike the bending case, when the flexible structure is under axisymmetric loadings, the contact issue only considers the normal contact but not the tangential, which has also been verified, for example, by Utting and Jones (1987) whose experiment discovers that the friction has little effect on the armoured spiral structure under tension. Dong, Zhang (Dong et al., 2013) and Guo, Chen (Guo et al., 2017) conducted a further study about the mechanical

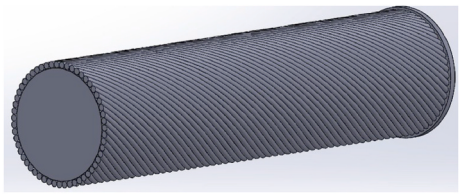

Fig. 2. Helical wires(Chang and Chen, 2019).

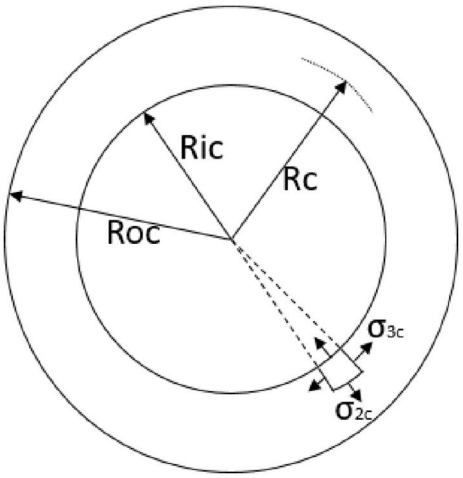

Fig. 3. Cross section of a cylinder.

$$\varepsilon_{1c}=\frac{u_z}{L},\varepsilon_{2c}=\frac{\partial u_{Rc}}{\partial R_c},\varepsilon_{3c}=\frac{u_{Rc}}{R_c},\varepsilon_{13c}=R_c\frac{u_{\theta c}}{L} \quad (1)$$

models of flexible pipes and umbilicals based on the principle of virtual work.

With the development of computers, the numerical method is more widely adopted in structure analysis. Some assumptions and restrictions of the theoretical method such as ignoring the friction and assuming plane cross-section can be eliminated. Both Sævik and Ekeberg (2002) and Skeie, Sødahl (Skeie et al., 2012) developed finite element programs named UFLEX and HELICA to predict the behaviour of flexible structures based on their analytical models by assuming that the friction-induced stick-slip only exist in the bending model. Knapp and Shimabukuro (2007) also developed a software CABLE CAD which can be adopted to analyse cross-section deformation caused by loads such as tension, bending and torsion. In addition, commercial three-dimensional finite element software such as ABAQUS and ANSYS are frequently used to proceed with the numerical study of flexible structures. For example, Chang and Chen (2019) adopted ANSYS to simulate the mechanical behaviour of a cable under tension as well as combined tension and external pressure, validating the tension stiffness derived from a simplified theoretical equation.

The mechanical study of flexible pipes and umbilicals has already been done by many previous scholars. For example, Bai's team conducted a series of analyses regarding fibre glass reinforced flexible pipes (Fang et al., 2018; Xu et al., 2019; Gao et al., 2019), steel strip reinforced flexible pipes (Fang et al., 2019; Bai et al., 2016b, 2017) and polyester reinforced flexible pipes (Sun et al., 2019). The study of umbilicals can also be easily found in the open literature(Bai et al., 2015). Current research of flexible structures mainly focused on one loading case. As power cables more and more used in deeper water areas with higher external pressure combined with other loadings, the mechanical behaviour of them under these combined axisymmetric loadings should be rigorously studied. An analytical method can give a more realistic mechanical response the simplified method fails to, for example, the geometry deformation of wires is found to be an important factor to influence the stiffness which the simplified equation fails to take into consideration(Chang and Chen, 2019).

This paper aims to investigate the mechanical behaviour of a power cable under axisymmetric loadings(including the most typical combined external pressure and tension) through analytical and numerical approaches. The principle of virtual work is applied in the analytical model to formulate the governing equations with the normal contact conditions and geometry nonlinearity introduced into the principle of virtual work. Section 1 introduces the background, research motivation and

objectives. Section 2 presents the analytical method of power cables with regard to cylinder and helical structures. Section 3 discusses the numerical model built through ABAQUS followed by Section 4 comparing and analysing the result from the analytical method and numerical method. Section 5 presents some parametric studies that are thought to matter the cable behaviour, proposing a cable design with better mechanical properties. The final section lists the conclusions found in this study.

2. Analytical study

As shown in Fig. 1, marine power cables usually consist of several layers made of different materials. The conductor, insulation, conductor screen and insulation screen belong to the dielectric system, which serves for electricity function. The other layers outside the dielectric system mainly provide the mechanical function and protect the inner layers. From the structural point of view, for the simplicity of the analytical derivation, a power cable consists of two basic structure styles. One is the cylinder structure such as the conductor and insulation layer, while the other is the armour layer, shown in Fig. 2, composed of numerous helical wires winding around the inner layers. The latter is a key element in deciding the mechanical response of power cables, as it provides both superior axial stiffness and bending flexibility. However, the study regarding it is complicated due to its structural style and complex contact with its neighbouring layers. However, some research Merino, de Sousa (Merino et al., 2009) has shown that friction has minor and negligible influence on the behaviour of flexible under axisymmetric loadings. The normal contact is reflected in the contact and detachability of the neighbouring layers in the normal direction, and this should be taken into consideration in the case of axisymmetric loadings. The following part of this section will introduce the analysis with regard to both cylinder structure and helical structure, then the analytical model of a whole cable under axisymmetric loadings considering the normal contact issue is given.

Before the analytical derivation, a few assumptions of cables under the axisymmetric loadings are given:

1. The geometry imperfection is not considered
2. The geometry deformation of each wire in the same layer is the same and there is a reserved distance among each wire. As a result, the normal contact among each wire in the same layer is not considered as these wires move together under axisymmetric loading.
3. Due to the significant axial and radial stiffness of power cables, the small deformation hypothesis is satisfied. Therefore, the materials used in the model are treated as elastic.

2.1. Cylinder

Cylinder structure under tension, torsion or external pressure can be regarded as both axisymmetric and plane strain problems. According to elastic mechanics, the cylinder would generate axial strain ε_{1c}, radial strain ε_{2c}, hoop strain ε_{3c} and shear strain ε_{13c}:where L is the length of one wire pitch which means the endpoint distance of the wire when it circulates completely one circle, u_z the axial displacement, $u_{Rc}$the radial displacement of the cylinder, $u_{\theta c}$ the rotation angle of this layer. The strain energy in the cylinder is:

$$\prod_{cu} = \frac{1}{2}\int_V \left(\sigma_{1c}\varepsilon_{1c} + \sigma_{2c}\varepsilon_{2c} + \sigma_{3c}\varepsilon_{3c} + \sigma_{13c}\varepsilon_{13c}\right) dV \tag{2}$$

The strain of isotropy material, based on generalized Hooke's law, is:

$$\sigma_{ijc} = \lambda\varepsilon_{kkc}\delta_{ij} + 2\mu\varepsilon_{ijc} \tag{3}$$

where λ and μ are called Lame constant, expressed by Young's modulus E and Poisson's ratio ν as:

$$\lambda = \frac{E\nu}{(1+\nu)(1-2\nu)}, \mu = \frac{E}{2(1+\nu)} \tag{4}$$

The total potential of the loads is:

$$\prod_{cw} = P_{ic}\Delta V_{ic} - P_{oc}\Delta V_{oc} + Fu_{zc} + Tu_{\theta c} \tag{5}$$

P_{ic} and P_{oc} are the internal and external pressure on the cylinder, respectively; F is the tension force and T is the axial torsion. ΔV_{ic} and ΔV_{oc} are the volume change of the inside and outside, they are expressed as follows:

$$\Delta V_{ic} = \pi R_{ic}^2 u_{zc} + 2\pi R_{ic} u_{Ric} L \tag{6}$$

$$\Delta V_{oc} = \pi R_{oc}^2 u_{zc} + 2\pi R_{oc} u_{Roc} L \tag{7}$$

u_{Ric} and u_{Roc} are the change of the radial displacement of the inner surface and the outer surface. The total potential energy (Bathe and Bathe, 2006) of the cylinder is:

$$\Pi_c = \Pi_{cu} - \Pi_{cw} \tag{8}$$

2.2. Helical wires

Since the wire layer is composed of numerous wires, this part will introduce how a single wire responds first, then the response of a wire layer will be discussed afterwards. There are two basic geometric parameters of a wire, the radius R and the winding angle α, shown in Fig. 4. α can be decided by $\tan\alpha = \frac{2\cdot\pi\cdot R}{L}$. Once the two parameters are confirmed, the structure style of the wire can be confirmed as well.

When a cable is under external loadings, wires will generate axial, bending and torsion strain, as well as radial strain. Based on the formula derived by Knapp (1979), the axial strain of a helical element is given by:

$$\varepsilon_1 = \frac{u_z}{L}\cos^2\alpha + \frac{u_R}{R}\sin^2\alpha + R\frac{u_\theta}{L}\sin\alpha\cos\alpha \tag{9}$$

where L and u_z are the same as the meanings in the cylinder, u_R the radial displacement, u_θ the rotation angle of the wire in winding direction.

The radial strain can be expressed as:

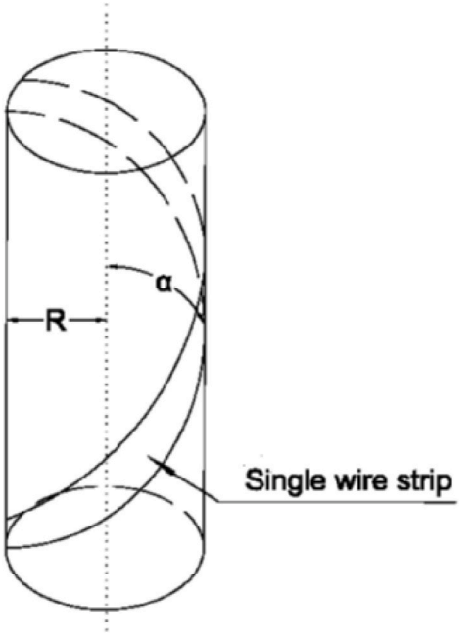

Fig. 4. Helical wires.

$$\varepsilon_2 = \frac{\Delta t}{t} \tag{10}$$

where t is the thickness of the wire, and Δt is the variation of the thickness.

The bending and torsion strain can be given after the moving reference frame is built for the wires. Frenet-Serret frame (Feret and Bournazel, 1987), as shown in Fig. 5, is used to reflect the curvature change in each direction. The orientation is such that G1 is the winding direction of the wire, while G2 is directed along the inward normal of the supporting surface, and G3 is determined by the right-hand rule. The change of bending curvature $\Delta\kappa_3$ and twist $\Delta\kappa_1$ based on Frenet-Serret frame and differential geometry are shown in following:

$$\Delta\kappa_3 = \frac{\sin^2\alpha'}{R'} - \frac{\sin^2\alpha}{R} \tag{11}$$

$$\Delta\kappa_1 = \frac{\sin\alpha'\cos\alpha'}{R'} - \frac{\sin\alpha\cos\alpha}{R} \tag{12}$$

Where α' and R' are the wire angel and radius after deformation. The change of wire angles in the wire layers can be calculated from the following equation proposed by Knapp (1979):

$$\cos\alpha' = \tan\alpha \frac{L(1+\varepsilon_{1c})}{\left\{[L(1+\varepsilon_{1c})]^2 + [2\pi R(1+\gamma)]^2\right\}^{1/2}} \tag{13}$$

In which:

$$\gamma = \frac{\varepsilon_{13c}}{\tan\alpha} \tag{14}$$

As for the total potential of the loads, the wire layer is composed of numerous wires which are closely contact with each other, and the behaviour of all the wires is assumed to be the same in the same layer. Therefore, the total potential of the loads of a wire layer can be expressed as the linear superposition of all the wires:

$$\prod_{ww} = P_i\Delta V_i - P_o\Delta V_o + Fu_z + Tu_\theta \tag{15}$$

where the definition of P_i, P_o ΔV_i, ΔV_o, F and T share the same meaning as their counterparts in the cylinder structure.

ΔV_i and ΔV_o can be expressed as:

$$\Delta V_i = \left(\frac{u_z}{L} + 2\frac{u_R}{R}\right)\pi R_i^2 L \tag{16}$$

$$\Delta V_o = \left(\frac{u_z}{L} + 2\frac{u_R}{R}\right)\pi R_o^2 L \tag{17}$$

The total strain energy of one single helical wire is:

$$\prod_{wu} = \frac{1}{2}\int_v (\sigma_1\cdot\varepsilon_1 + \sigma_2\cdot\varepsilon_2 + EI_3\cdot\Delta\kappa_3^2 + GJ\cdot\Delta\kappa_1^2)dv \tag{18}$$

where I_3 is the moment of inertia in the G3 direction in Fig. 5; G is the shear modulus of the wire; J is the polar moment of inertia. The domain of integration is the wire with one pitch length. σ_1 and σ_2 are the axial stresses in G1 and G2 direction, respectively, and disregarding the contribution from the curvature, they can be described as:

$$\sigma_1 = \frac{E}{1-\nu^2}(\varepsilon_1 + \nu\varepsilon_2), \sigma_2 = \frac{E}{1-\nu^2}(\varepsilon_2 + \nu\varepsilon_1) \tag{19}$$

$\nu$is the Poisson's ratio of the wire.

From Eq.(13) and Eq.(16), the total potential energy of the wire layer can be expressed as:

$$\Pi_w = n\cdot\prod_{wu} - \prod_{ww} \tag{20}$$

where n is the amount of the wires in the layer.

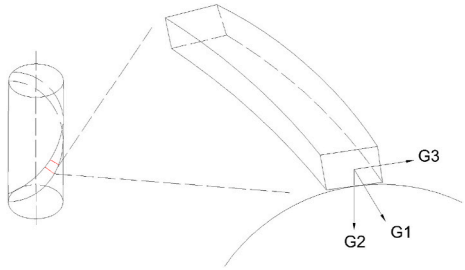

Fig. 5. Definition of frenet-serret.

2.3. Solution method

Considering that power cables are a type of multi-layer structure, the neighbouring layers might contact or separate in the normal direction under axisymmetric loadings, therefore, the contact issue inside power cables should be taken into account in the analytical model. In this way, the cylinder layer and wire layer are deformation compatible and force-balanced.

The neighbouring layers would separate if the contact pressure is negative, otherwise, they are contacting each other. Based on the constraint variation principle, additional variation should be added when the constraint is considered so that a correction functional is constituted. Two widely used procedures are available, namely the Lagrange multiplier method and the penalty method (Sævik and Gjøsteen, 2012). Both of them operate on the variational or weighted residual formulations of the problem to be solved (Bathe and Bathe, 2006). Compared with Lagrange multiplier method, the penalty method does not increase any additional degree of freedom(DOF) of the system. The coefficient matrix remains positive, which facilitates the solution to the matrix. Therefore, This paper chooses the penalty function to impose the constraints generated by the contact. The total potential energy can be expressed as:

$$\Pi = \Pi_s + \Pi_p \tag{21}$$

where Π_s is the total potential excluding the energy caused by contact, which is $\Pi_s = \Pi_c + \Pi_w$, while Π_p is the additional function by introducing the contact condition. When the neighbouring layers contact:

$$\Pi_{p1} = \sum_{j=1}^{m-1}\left[\omega_{ju}\left(u_{jRo} - u_{(j+1)Ri}\right)^2 + \omega_{jp}\left(P_{jo} - P_{(j+1)i}\right)^2\right] \tag{22}$$

where j is the layer order of the cable(m layers in total); ω_{ju} and ω_{jp} are the penalty parameters of j-th layer, which are constants of relatively large magnitude; u_{jRo} is the radial displacement of the outer surface of the j-th layer; $u_{(j+1)Ri}$ is the radial displacement of the inner surface of the (j+1)-th layer; P_{jo} and $P_{(j+1)i}$ are the external pressure of the j-th layer and the internal pressure of the (j+1)-th layer.

Once the neighbouring layers are separate, the contact pressure becomes zero, and the radial displacement is no longer continuous, therefore, the additional function becomes:

$$\Pi_{p2} = \sum_{j=1}^{m-1}\left[\omega_{ju}P_{jo}^2 + \omega_{jp}P_{(j+1)i}^2\right] \tag{23}$$

Based on the principle of minimum potential energy, the exact solution to all possible displacements leads to the minimum potential energy of the system. Therefore, taking a variational of the total potential energy and letting it equal to zero, either: when the neighbouring layers are in contact

$$\delta\Pi = \delta\Pi_s + \delta\Pi_{p1} = 0 \tag{24}$$

Or, when the neighbouring layers are detached

$$\delta\Pi = \delta\Pi_s + \delta\Pi_{p2} = 0 \tag{25}$$

According to the above equations, the matrix equations can be obtained:

$$[K]\{\Delta_s\} = \{F_s\} \tag{26}$$

where [K] is the 2m + 2 by 2m + 2 stiffness matrix, in which m is the total layer amount of the cable, $\{F_s\}$ is the vector of the external loadings and $\{\Delta_s\}$ is the displacement vector, including an axial displacement, a rotation angle as well as radial displacements of each layer. In order to solve these equations, necessary parameters, e.g., geometry, material, loadings and boundary conditions, should be inputted firstly. The main steps of the calculation procedure executed in software MATLAB is shown in Fig. 6.

The above section introduced the analytical derivation of power cables and gave the analytical solution to them. The following part will present the numerical simulations and it will verify the analytical solution.

3. Numerical simulations

In this part, a finite element model(FEM) is established in ABAQUS to study the mechanical behaviour of cables subject to axisymmetric loadings. The cable built in this paper, shown in Fig. 7, is based on the data provided by Panza (2020), in which the geometry and material parameters are given, as shown in Table 1 and Table 2. The wires constituting Layer Ⅴ and layer Ⅶ share a rectangular shape with the width and thickness as 6 mm and 3 mm, respectively. The amount of the wires and the winding angle in Layer Ⅴ are 52 and 12.7deg, while the values for Layer Ⅶ are 56 and -10.5deg.

Three different lengths, 1m, 3m and 6m, are chosen to model the cable at first and the tension stiffness and torsion stiffness are found to be almost the same, with an error of less than 1%, proving the length does not have much influence on the final result. In order to save computation time, the cable used in the following analysis has a length of 1m. Fig. 8 shows the three-dimensional model of the cable with regard to its front view, side view, as well as the side view of the helical wire layers.

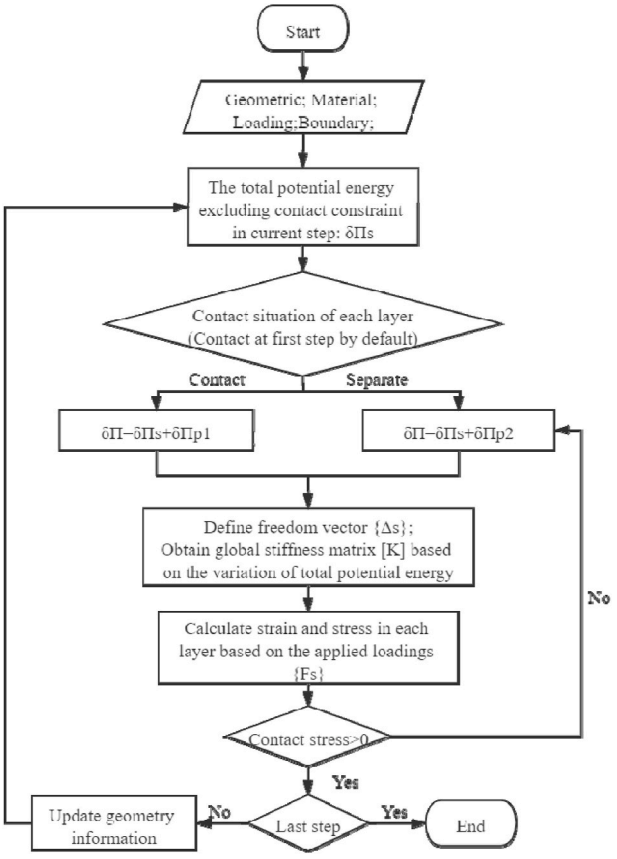

Fig. 6. Flow chart of analytical solution procedure for cable.

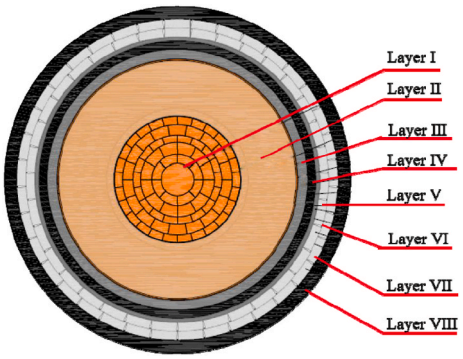

Fig. 7. Cross section of the target cable.

Table 1
Size chart of the power cable.

No.	Component	Thickness(mm)	Outer Diameter(mm)
Layer I	Conductor	–	23.55
Layer II	Insulation	21.05	44.6
Layer III	Lead sheath	3.3	47.9
Layer IV	PE sheath	3.6	51.5
Layer V	Armour layer	3	54.5
Layer VI	Bedding	0.5	55
Layer VII	Armour layer	3	58
Layer VIII	Outer sheath	6	64

Table 2
Material properties.

No.	Elastic modulus(Mpa)	Poisson ratio
Layer I	1.2e5	0.34
Layer II	1.93e4	0.44
Layer III	12000	0.43
Layer IV	600	0.46
Layer V	2e5	0.3
Layer VI	301	0.45
Layer VII	2e5	0.3
Layer VIII	780	0.46

3.1. Mesh and interaction

C3D8R element (eight-node continuum linear brick elements with reduced integration and hourglass control) is selected for the cylinders

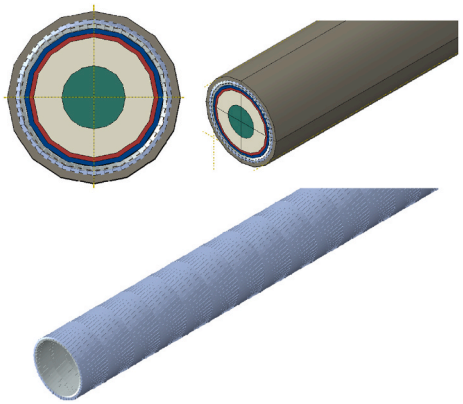

Fig. 8. Finite element model of the power cable.

and the middle conductor, which is able to reflect the variation of wall thickness and stress distribution with efficient computation without losing the accuracy (Abaqus, 2014). The helical wires are modelled by beam elements(B31). This type of element is a 2-node linear beam based on Timoshenko beam theory, able to capture the axial stress and bending moments of the beam. Besides, it is much more efficient than solid element with regard to the computation time when numerous wires are simulated within a cable. In addition, the size of the mesh is correlated with the accuracy and computational time of the simulation results. Two different mesh sizes are tested, as shown in Fig. 9. The simulated tensile stiffness based on the coarse mesh and the fine mesh size are 6.44e8N/mm and 6.39e8N/mm respectively, and the corresponding torsional stiffnesses are 1.07e11 N mm/rad and 1.03e11 N mm/rad, respectively. The error between two mesh sizes regarding both tension stiffness and torsion stiffness is less than 0.78%, therefore, the coarse mesh size is used in the study.

The interaction between each layer is simulated as general contact. Depending on the contact pressure between two neighbouring layers, ABAQUS will judge and identify all possible contact pairs, including all of the solid components and the helical wires. The normal mechanical behaviour is defined as “Hard Contact” with ”Allow separation after contact.” “Hard Contact” means the magnitude of the contact pressure between two neighbouring layers is unlimited when they are in contact. The neighbouring layers will separate when the value of the contact pressure less than or equal to zero, and the contact restriction on corresponding points will be set free since. The tangential behaviour is set as frictionless for the case of tension, as well as the case of combined tension and external pressure. This means friction coefficient is set to zero among all of the components within the cable, and thus each component is free in the tangential direction.

3.2. Load and boundary conditions

In order to ensure that the boundary conditions are the same as those in the analytical model, one end of the FE model is totally fixed, while the other is coupled to a reference point RP1, located at the centre of the bottom end. DOFs of this cross section in all directions are coupled with this point so that all layers and the end points of the wires are connected rigidly to this reference node. Three loading conditions are simulated in this paper and their boundary conditions are shown in Table 3. A tension force is applied in z-direction for tension case; A torsion is applied in the z-direction for torsion case; Except the axial force in the z-direction, extra average external pressure is applied on the outmost layer for the combined case. Fig. 10 presents an illustration of the tension case.

4. Discussion of the results

Three loading cases were described in section 3.2. The following part will discuss the results corresponding to each case one by one.

4.1. Tension

In the tension case, a tensile force 3e6N is applied to the left reference point. “Dynamic implicit” procedure is activated to efficiently

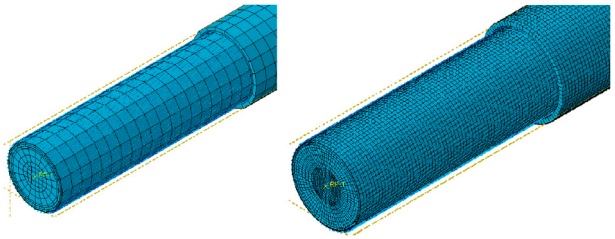

Fig. 9. Meshing of beam and solid elements with two different mesh sizes.

Table 3
The boundary conditions for three loading cases.

DOF	Tension/combined tension and external pressure		Torsion	
	Left	Right	Left	Right
x	1	1	1	1
y	1	1	1	1
z	0	1	1	1
x-rot	1	1	1	1
y-rot	1	1	1	1
z-rot	0	1	0	1

• 1 means the corresponding DOF is fixed; 0 means it is free.

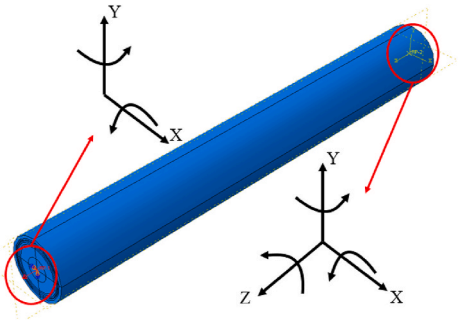

Fig. 10. Load and boundary conditions of cables subject to tension.

achieve relatively accurate quasi-static analysis results in the numerical model, where the step time should be a factor of 10–50 times slower than the fundamental frequency of the structure in order to reach a quasi-static result (Abaqus, 2014). In order to ensure the result is reasonable, the ratio between kinetic energy(ALLKE) and strain energy (ALLSE) for the whole model should be low enough during the simulation process. As the energies illustrated in Fig. 11, the kinetic energy (ALLKE) is far smaller(less than 5%) than that of strain energy(ALLSE), confirming the availability of the calculated results. The following simulations are also checked in the same way with regard to the energy ratio without repeat again for the simplicity of the paper.

Fig. 12 shows the largest axial strain appears near the area where the tensile force is applied, while the smallest axial strain locates at the fixed ending. The final deformation of the wires in LayerⅤ and LayerⅦ, shown in Fig. 13 and Fig. 14, illustrates the wires are still attaching with their inner layer during the simulation without apparent slip. These two images will compare with the final deformation of the wires under torsion, and obvious difference will be observed. Fig. 15 shows the axial strain-tension force relationship from these two methods. It can be

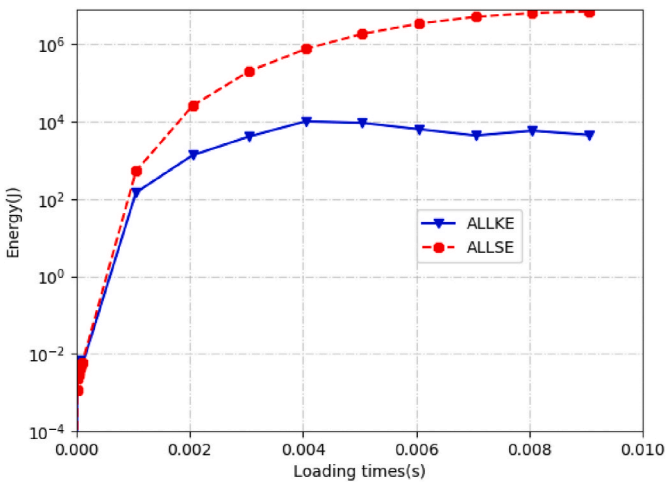

Fig. 11. Energy distribution of the FEM.

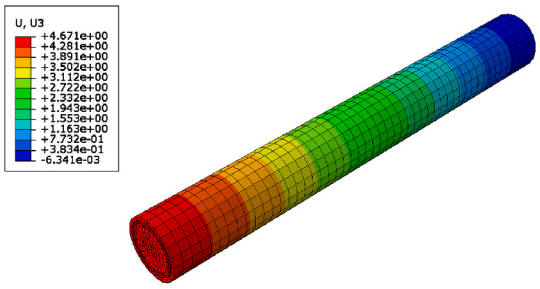

Fig. 12. Axial displacement distribution of the cable under tension.

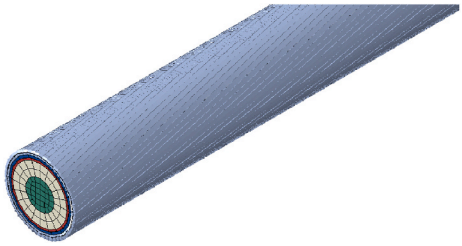

Fig. 13. The final deformation of the wires in LayerⅦ under tension.

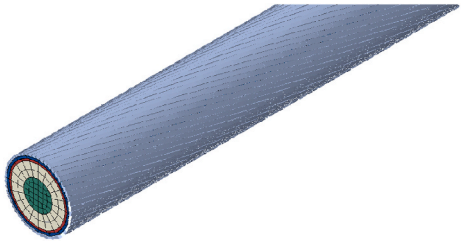

Fig. 14. The final deformation of the wires in LayerⅤ under tension.

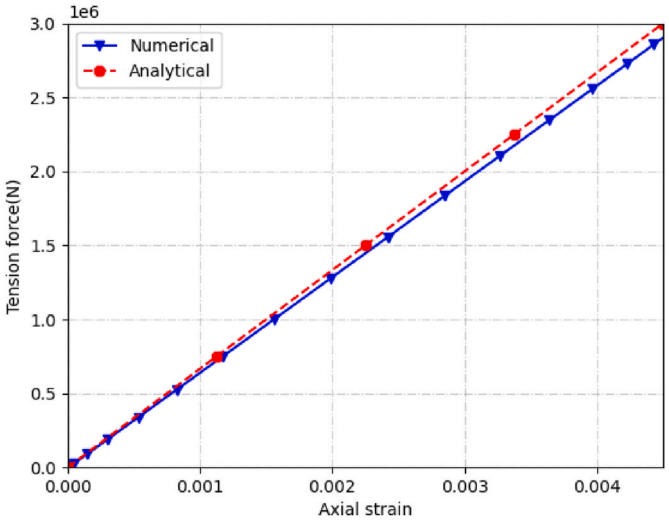

Fig. 15. Axial strain-tension force relationship from analytical and numerical methods.

observed that the mechanical response of the cable under tension is highly linear even though the analytical formulae are nonlinear. The tensile stiffness(the slope of the curve) from the analytical model is 3.3% higher than that from the numerical model, illustrating the stiffness from these two methods agree quite well with each other. The difference is likely to be caused by the fact that the numerical solution considers the curvature change in the G2 direction(Fig. 5) while the analytical solution does not. Besides, the integral behaviour of the cable is assumed as a superposition of all the components and the contact in the tangential direction is not considered in the analytical solution.

In order to study the stress distribution of the cable under tension, Fig. 16 shows the stress distribution of the cross section of the cable under tension. As can be seen from the colour bar in the figure, the wire layers of the cable are the primary part withstanding the axial force. In fact, the Sensitivity study in this paper shows the stiffness between the cable and a cable without wires reaches a difference of 53.18%, which means the wires play a significant role with regard to the tension behaviour.

Since armour is the main part resisting the load, the stress distribution of the steel wire under tension is further studied. In order to eliminate the boundary effect, the middle part of the cross section, as shown in Fig. 17, is then cut out. It can be seen from Fig. 18 and Fig. 19 that the axial stress distribution in each point of each wire in both LayerⅤ and LayerⅦ is not exactly the same, and the difference between the maximum and minimum wire stress in LayerⅦ has a larger difference than that in LayerⅤ. The reason for the different distribution of the stress is that the contact situation between each wire and its neighbouring layer is not the same, as shown by the contact stress under two different axial strains in Fig. 20 and Fig. 21, which represent the contact stress applied by their neighbouring layers. It is obvious that the contact stress distributes randomly along these wires. This phenomenon can be caused by the initial geometry difference during the modelling process. Since the wires are complex curve beam, even though they are built as much as possible to contact perfectly with their neighbouring layers, ABAQUS can not guarantee there is no any gaps among structures. Besides, during the deformation process, the mesh distortion of each point of a wire corresponding to the mesh distortion of its neighbouring layers is not the same either. The mesh size of each component can also influence the stress distribution. Theoretically, the stress distribution can be average if the mesh is fine enough, however, that would cost a lot of computation. Considering the practical situation in real life, each wire shares a different geometry and various contact issue, there is definitely difference of the stress among each point of each wire as well. Therefore, an average stress of all the wires is more pragmatic and deserves more attention if we want to evaluate the stress of the wires. The stresses of all the wires from Figs. 18 and 19 are extracted and the average value of them is obtained. The average axial stress are 871Mpa and 853Mpa of the wires in LayerⅤ and LayerⅦ, respectively, only 0.62% and 1.80% higher than the results from the analytical model. The corresponding values from a finer-meshed model are also extracted and they are 869Mpa and 852Mpa of the wires in LayerⅤ and LayerⅦ with a difference of 1.5%. Therefore, it can be observed that the coarse mesh is enough to generate an accurate axial stress. As the torsion DOF of the left side is not restricted, the torsion angle of this side is also checked. The

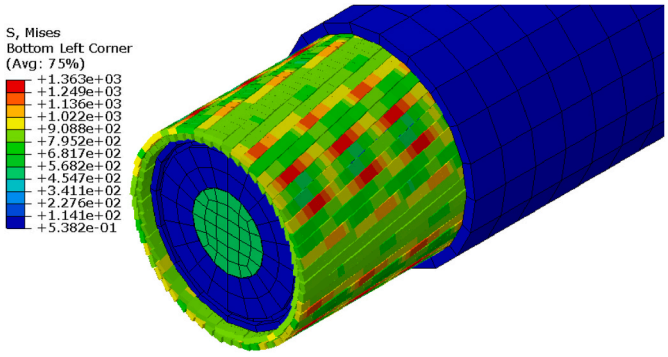

Fig. 16. The final Mises stress distribution of the cable cross section under tension.

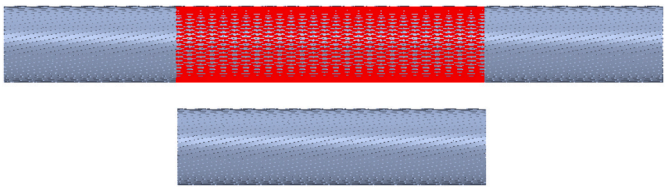

Fig. 17. Middle part of the helical wire layer.

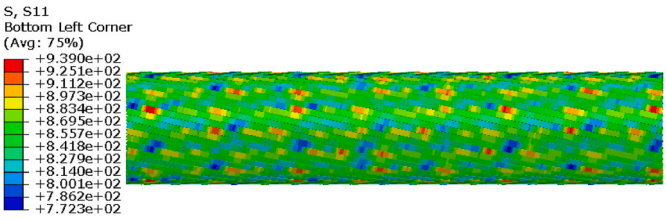

Fig. 18. Axial stress distribution in LayerV.

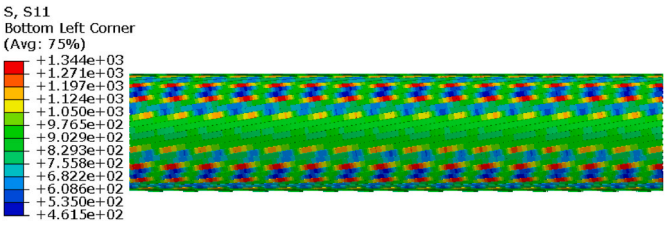

Fig. 19. Axial stress distribution in LayerⅦ.

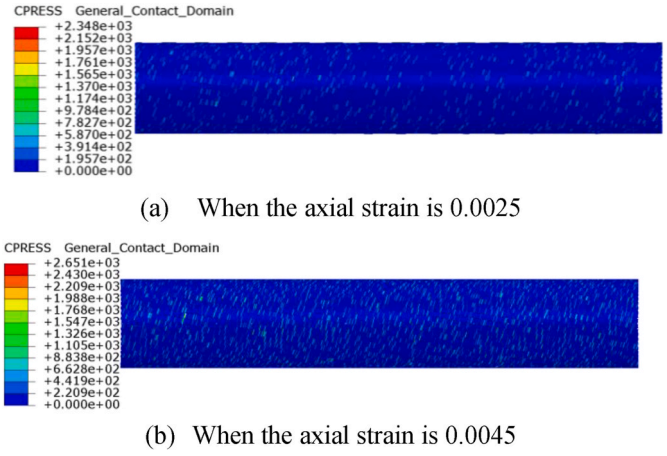

Fig. 20. Contact stress distribution of wires in LayerV when the axial strain of the cable are 0.0025 and 0.0045.

rotation angles from ABAQUS and the analytical model are 3e-7rad and 1.96e-06 rad, respectively, illustrating the rotation angle does not have a noticeable change under tension.

4.2. Torsion

Longva and Sævik (2016)gave different failure modes and presented three different mechanisms provoking torsional failure of flexible pipes. Fang, Xu (Fang et al., 2018) and Fang, Yuan (Fang et al., 2019) studied the failure styles of fibre glass flexible pipes and metallic strip flexible pipes under torsion. Power cables encounter torsion loading as well in practical engineering. In order to predict the torsion stiffness of the target cable, the mechanical response of the cable under torsion in two

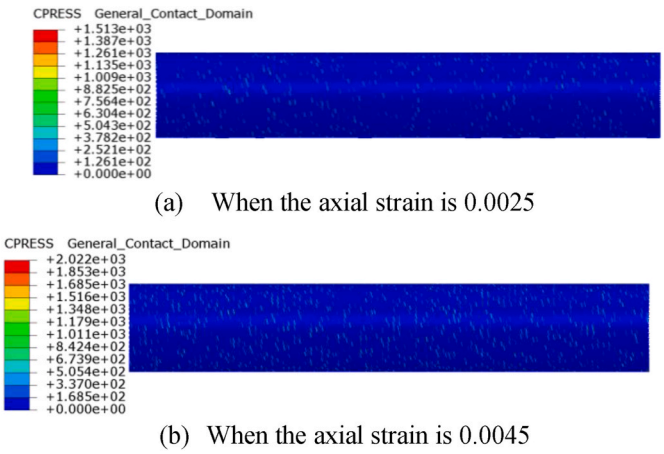

Fig. 21. Contact stress distribution of wires in LayerⅦ when the axial strain of the cable are 0.0025 and 0.0045.

directions(anti-clockwise and clockwise) will be shown in the following.

In the first case, an anti-clockwise torsion force 1e8N·mm is applied to the left reference point. Two simulation schemes are tested here. The first one takes the transverse contact as frictionless which means the contact surfaces are free to move away from each other, while the other one takes it as rough which means the contact surfaces stick together in the tangential direction during the simulation. The practical situation should stay between these two schemes, i.e., the friction efficient is between frictionless and rough. Fig. 22 shows the twist angle-torque relationship from these two methods, while the numerical includes two schemes mentioned just now. The stiffness from the analytical model is found to be higher than that from the numerical model, which might be caused by the fact that the analytical model fails to consider the curvature change in the G3 direction. Besides, the friction is found to have a considerable influence on the cable behaviour under this loading case. It can be observed that the mechanical response of the cable under torsion is linear from the analytical method and the numerical method with rough contact. As for the frictionless situation, the behaviour of the cable is linear when the twist angle is less than 0.00027 rad/mm, however, when it surpasses that value, the curve turns in a different style. In order to check out what happens inside the cable, picking out a time point when the twist angle is 0.00027 rad/mm, the outmost layer is removed and the deformation of the wires in LayerⅦ is shown in Fig. 23. It is clear that the wires slip away from their original location and obvious deformation can be observed. In fact, 0.0027 rad/mm is

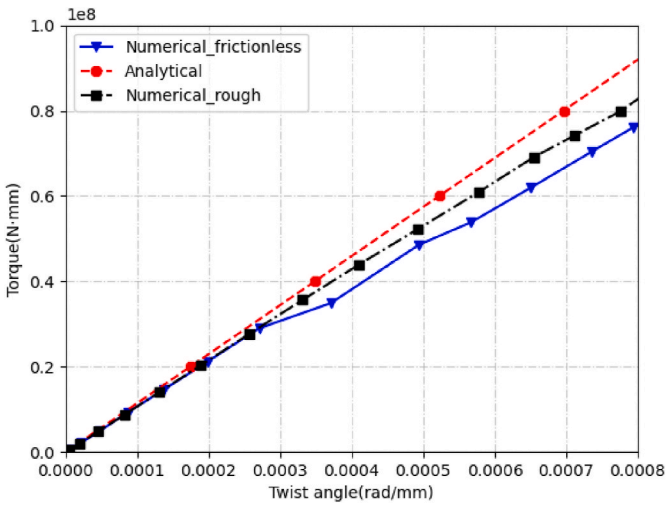

Fig. 22. Twist-torque relation of the cable under anti-clockwise torque.

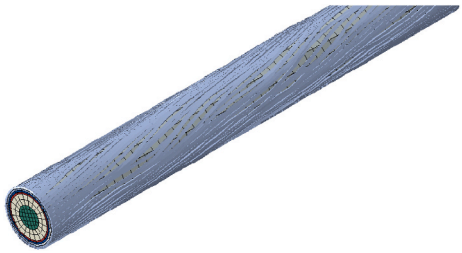

Fig. 23. The deformation of the wires in LayerⅦ under anti-clockwise torque with frictionless contact after slip.

exactly the critical point when the slip happens. The wires are still attached to the inner surface when the twist angle is less than this value. The wires in LayerVis also extracted out to check out the deformation, as shown in Fig. 24, and they are found to keep on attaching with the inner layer during the simulation. This can be compared with the deformation of the two wire layers in the tension case, shown by Figs. 13 and 14. The reason for this different phenomenon in two wire layers under torsion is that the wires in LayerⅦ mainly bear compression as they are winding around in the opposite direction with the torque direction, while the wires in LayerⅤ mainly bear tension for they are winding around in the same direction as the torque direction. The stiffness error between the numerical method and analytical method before the slip appears is 6.72%. In addition, the final Mises distribution in Fig. 25 shows, like the tension case, that the wires are the major parts to withstand the torque as well.

Same as the manipulation in last section, the stress in the middle part of all the wires in LayerⅤ and LayerⅦ are obtained respectively when slip is about to appear. Noteworthy, the layer with the winding angle same as the torque(LayerⅤ) presents positive tension stress while the stress of the wires winding in the opposite direction(LayerⅦ) is negative, which again means under torque, one wire layer is pulled, the other wire layer is compressed, as shown in Table 4. The error for both layers is less than 1.65%.

In the clockwise case, two transverse contact schemes are simulated here as well. Like the anti-clockwise case, the twist angle-torque relation of the three curves shown in Fig. 26 presents a similar trend, i.e., there is a turning point of the numerical curve when the transverse is considered as frictionless, which is also when the wires begin to slip. The deformation of the wires in LayerⅦ and LayerⅤ at this turning point, shown in Fig. 27 and Figs. 28 and 29, are observed to have the exact opposite deformation style as their counterparts under anti-clockwise torque.

The stiffness error between the numerical and analytical method before the slip occurs is 6.73% from the twist angle-torque relation in Fig. 26. The difference in the torsion stiffness of the cable under two directions from the analytical model is 1.42%, illustrating the torque direction hardly influences the torsion stiffness of the cable. The average stress of all the wires in the middle 500 mm of both layers when the slip is about to happen, similarly, is shown in Table 5. The error for both layers is less than 2.63%.

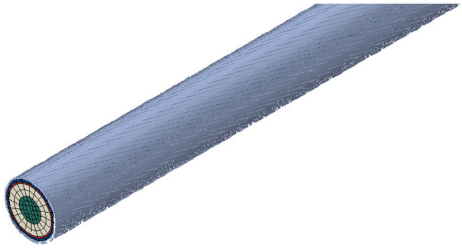

Fig. 24. The deformation of the wires in LayerⅤ under anti-clockwise torque with frictionless contact after slip.

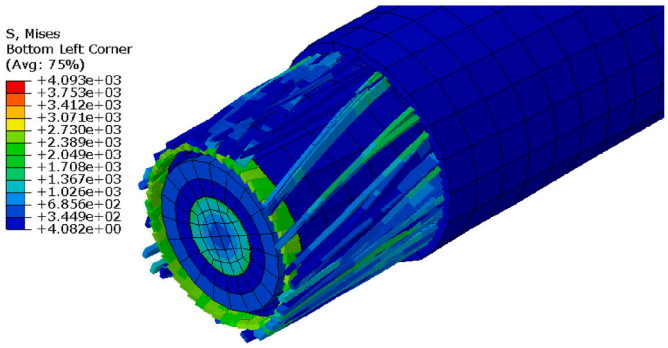

Fig. 25. The final Mises distribution of the cable under anti-clockwise torque.

Table 4
Wire stress along axial direction under anti-clockwise torque (Unit(Mpa)).

	Layer Ⅴ	Layer Ⅶ
Numerical	581.3	−492.3
Analytical	571.4	−488.1

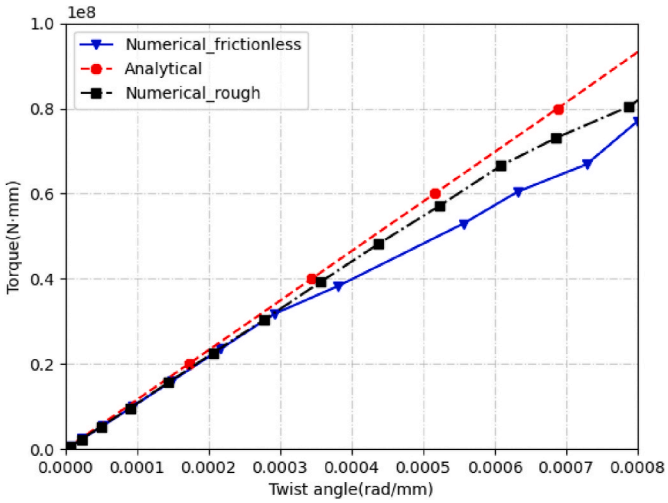

Fig. 26. Torque-twist angle relation between theoretical and numerical under clockwise torque.

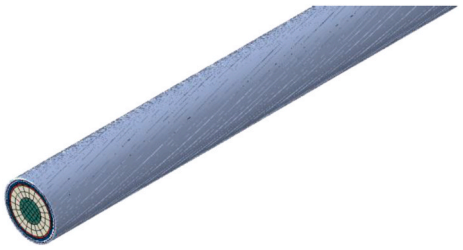

Fig. 27. The deformation of the wires in LayerⅦ under clockwise torque with frictionless contact after slip.

4.3. Combined external pressure and tension

In the deep-sea areas, submarine power cables are subject to not only tension, but also external pressure. The water pressure has been illustrated to have a significant influence on the behaviour of flexible pipes (Cornacchia et al., 2019). This part will verify the analytical model of submarine power cables under combined external pressure and tension.

Fig. 28. The deformation of the wires in LayerV under clockwise torque with frictionless contact after slip.

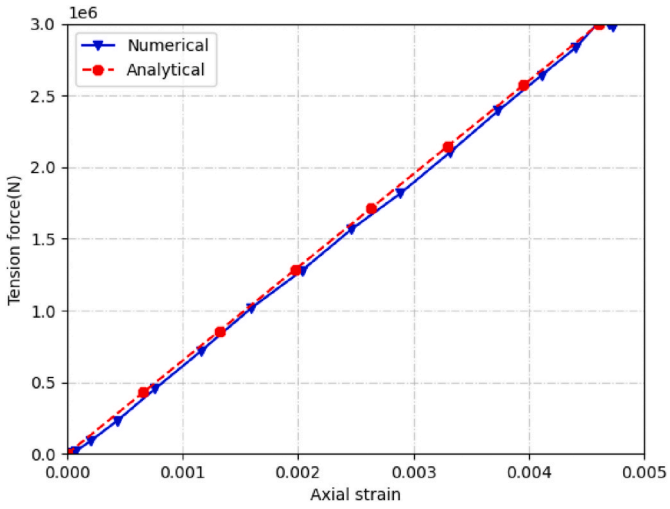

Fig. 29. Axial strain-tension force relationship under combined tension and external pressure from theoretical and numerical methods.

Table 5
Wire stress along axial direction under clockwise torque (Unit(Mpa)).

	Layer V	Layer VII
Numerical	−566.2	545.1
Analytical	−551.1	534.9

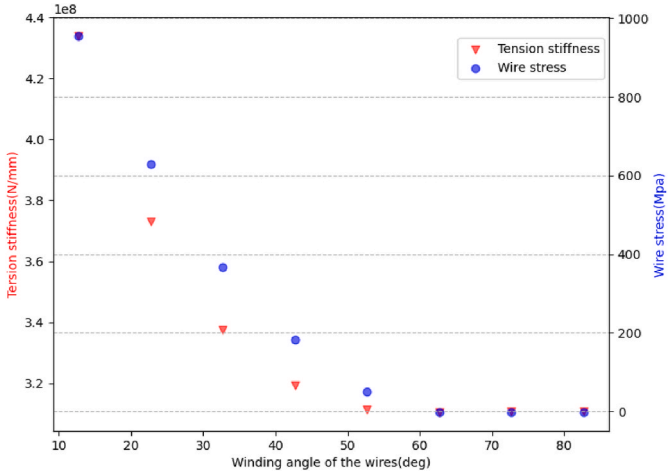

Fig. 30. Tension stiffness and wire stress under different winding angle with tension.

A tension force of 3e6N and an external pressure 4.9Mpa corresponding to 500m water depth are applied here.

Fig. 30 shows the axial strain-tension force relationship under combined tension and external pressure, where the numerical method and theoretical method agree with each other quite well. The stiffness under this situation is found 1.84% less than that under pure tension. The average stress of all the wires in the middle section in Layer V and layer VII is shown in Table 6. The error for both layers is less than 1.5%.

5. Parametric study

In this part, factors influencing the mechanical behaviours of power cables under axisymmetric loadings are investigated by the analytical model, including the effect of the external pressure. Other parameters should stay still while only one of them is changed in this analysis.

5.1. *Effect of winding angle*

The winding angle of the wire is a basic parameter, playing a key role in cable design. According to the results of the analytical analysis, the influence of winding angles on cable stiffness is considerable. Each cable design has a specific winding angle in order to obtain the optimized stiffness. In this section, the influence of the winding angle on the overall behaviour of the power cable is analysed. To simplify the analysis and better understand what is the effect of the winding angle, only the inner wire layer is kept in this section and changed from 12.7deg to 82.7deg with an interval of 10deg, while the outer wire layer is replaced and refilled by the outer PE.

The effect of the winding angle on the tension behaviour and torsion behaviour in two directions are studied here. Tension force 3e6N, torque 1e7N·mm and torque -1e7N·mm are applied on the end fitting, respectively. The stiffness of the whole cable and the wire stress under three situations are shown in Fig. 31, Fig. 32 and Fig. 33, respectively. It is clear with the increase of the winding angle, the tension stiffness and the wire stress is decreasing simultaneously. In this situation, the other layers would take more responsibility to bear the tension force, which is simple to be explained based on the stress resolved in two directions. As shown in Fig. 34, the stress resolved in the axial direction contributes to the tension stiffness while the stress resolved in the hoop direction contributes to the torsion stiffness. As the winding angle increases, the wire stress itself is decreasing, the stress resolved in the axial direction is decreasing as well. Thus the tension stiffness is decreasing as well, which is reflected in Fig. 31. As for the situation of clockwise torque, the wires have an optimized angle near 52.7deg where the torsion stiffness is the largest. When the winding angle changes from 52.7deg, the torsion stiffness decreases. The wire stress has a maximum value when the winding angle is near 22.7deg, however, it is not corresponding to the maximum torsion stiffness as the stress in the hoop direction does not reach a maximum value until the winding angle turns to 52.7deg. In the last case, when a torque is applied in the anti-clockwise direction, the wires are no longer tensioned but compressed. With the increase of the winding angles, the absolute value of the compressed wire stress is decreasing whereas the torsion stiffness is increasing firstly then decreasing after 22.7deg. This can be explained as well by the hoop stress resolved by the wire stress.

5.2. *Effect of wire layers*

Helical wires provide the majority of mechanical resistance for the

Table 6
Axial force along axial direction (Unit(Mpa)).

	Layer V	Layer VII
Numerical	852.6	871.05
Analytical	850.9	879.9

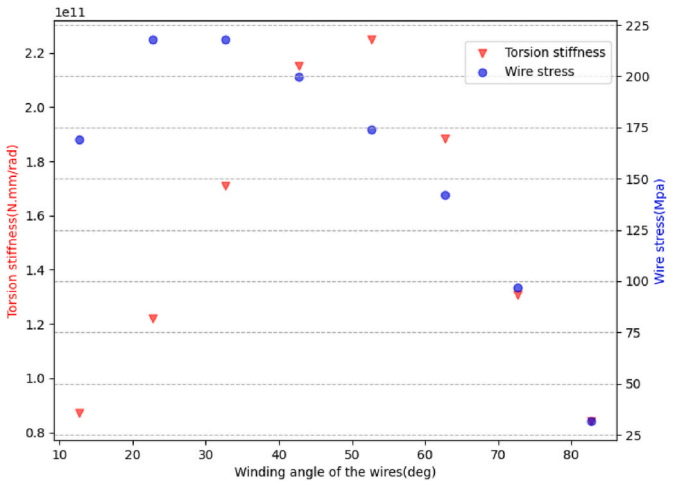

Fig. 31. Torsion stiffness and wire stress under different winding angle with clockwise torque.

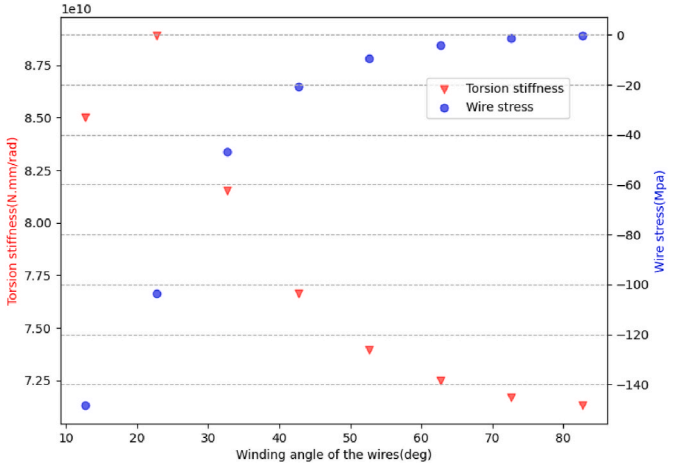

Fig. 32. Torsion stiffness and wire stress under different winding angle with anti-clockwise torque.

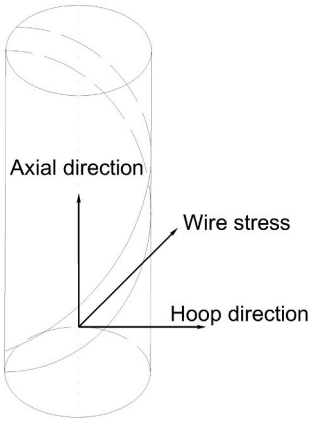

Fig. 33. Wire stress resolved in two directions.

cable under axisymmetric loadings. It is necessary to choose the cable with multi-layer wires in specific cases when large loadings are applied, likewise, considering the cost and the weight of the cable, single layer wires or double layer wires are preferred in some cases when loading is not a serious issue. The following part studies the influence of the

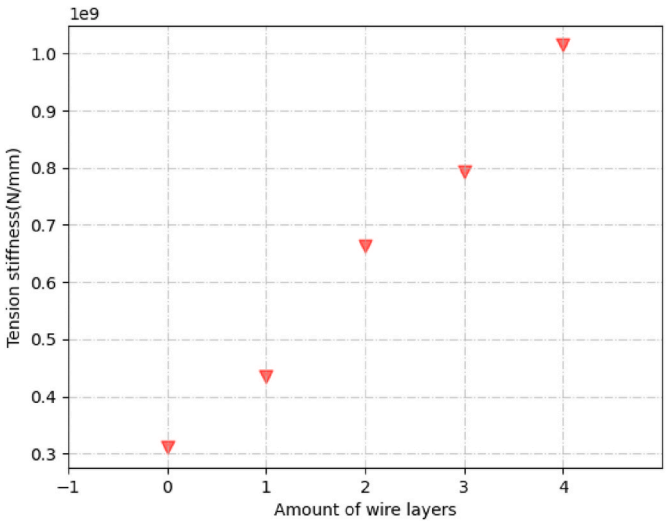

Fig. 34. The tension stiffness of the cable when the wire layers is changed from 0 to 4.

number of wire layers on the mechanical behaviour of power cables with regard to tension and torsion. Same as Section 5.1, tension force 3e6N, torque 1e7N·mm and torque -1e7N·mm are applied on the end fitting, respectively. Figs. 34 and 35 and 36 show the change of tension stiffness and torsion stiffness when the amount of wire layers changes from 0 to 4.0 means there is no any wires within the cable, although this might not be practical in reality, this case is studied here for the comparison purpose. It is obvious with the increase of the number of wire layers, all of the stiffness is increasing. The layers of the wire have a significant influence on the behaviour of the cable. It is also observed when there are no wires in the cable, a tension of the cable would not generate any torsion, and torsion of the cable would not generate any tension either, which means tension and torsion are decoupled in this case.

As for the axial stress in the wires, the results are shown in Table 7, Table 8 and Table 9. It is clear in the tension case, when the amount of the wire layers increases, the value of stress borne by each wire decreases as they would share the total stress together. In addition, the stress directions of the wires in the neighbouring layers are contrary in the torsion case, indicating one layer is pulled, the other layer is compressed.

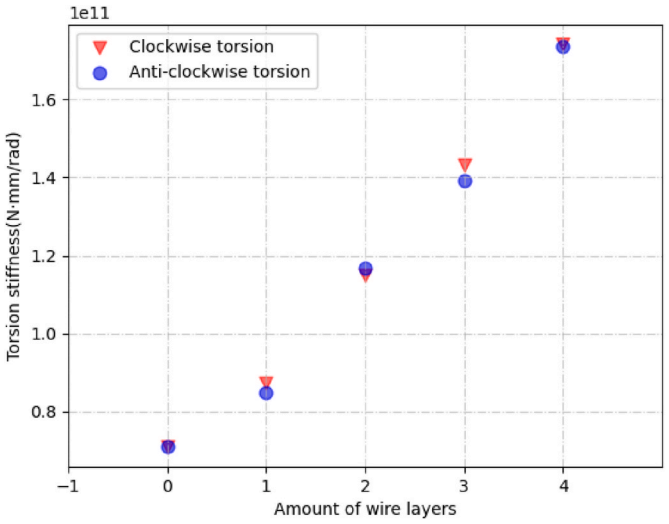

Fig. 35. The torsion stiffness of both directions of the cable when the wire layers is changed from 0 to 4.

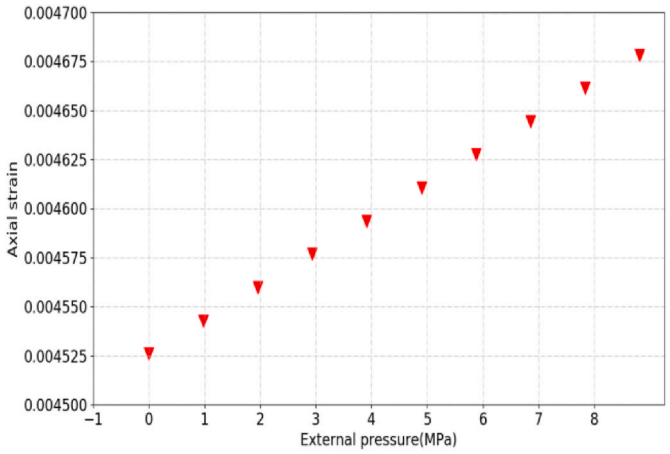

Fig. 36. The effect of external pressure on the axial strain.

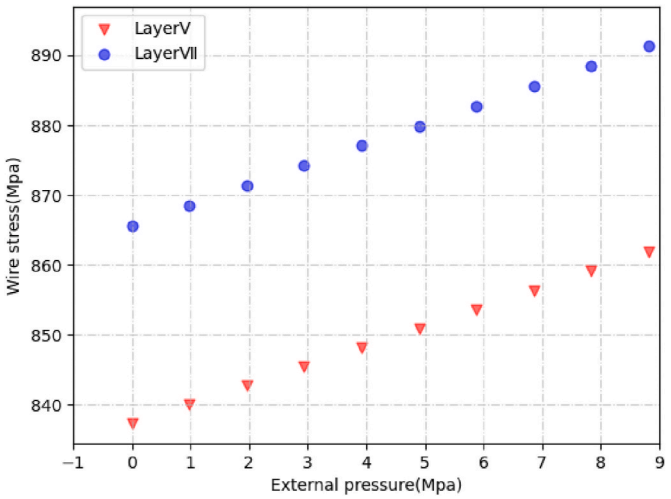

Fig. 37. Wire stress in LayerV and Layer VII.

Table 7
The stress of wires in each layer under tension (Unit(Mpa)).

	1 wire layer	2 wire layers	3 wire layers	4 wire layers
1st wire layer	955	837	569	544
2nd wire layer	–	865	841	566
3rd wire layer	–	–	551	544
4th wire layer	–	–	–	567

Table 8
The stress of wires in each layer under clockwise torsion(Unit(Mpa)).

	1 wire layer	2 wire layers	3 wire layers	4 wire layers
1st wire layer	169	190	122	127
2nd wire layer	–	−163	−179	−120
3rd wire layer	–	–	143	144
4th wire layer	–	–	–	−121

Table 9
The stress of wires in each layer under anti-clockwise torsion(Unit(Mpa)).

	1 wire layer	2 wire layers	3 wire layers	4 wire layers
1st wire layer	−148	−184	−136	−119
2nd wire layer	–	178	181	120
3rd wire layer	–	–	−127	−139
4th wire layer	–	–	–	133

5.3. Effect of external pressure

Submarine power cables now head into deeper water areas where higher external water pressure applies on the outside of them, inducing the cable response differently. In this section, the power cable under coupled tension and external pressure is analysed. Fig. 37 shows the relationship between axial strain and incremental external pressure. The external pressure is calculated based on the water depth the cable is deployed in, from 0 to 1000m at an interval of 100m here. It can be observed that with the increase of the external pressure, the axial strain is becoming higher. The difference in the axial strain of the cable under 0m and 1000m is 3.61%, indicating the external pressure does not have a large influence on this type of cable. A possible reason for this is that the cable studied in this paper is a solid structure with enough radial stiffness. It would not generate large radial deformation even though under deep waters. The situation is different if the flexible structure is an umbilical or a flexible pipe with a hollow interior. For example, Cornacchia, Liu (Cornacchia et al., 2019) shows that without a radial resistant pressure armour layer, the strength of the axial resistance is weakened significantly. Fig38 illustrates that with the increase of the external pressure, the wire stresses in both inner and outer wire layers become higher.

6. Conclusions

In this paper, the mechanical behaviour of submarine power cables subject to axisymmetric loadings is investigated by both analytical and numerical methods. The relationship between axial strain and axial force, as well as the torsion angle and torque for the cable acquired from the analytical method show good agreement with the ones obtained from simulations. Besides, the stress given by the analytical model enables engineers to have a rough estimation of the wire behaviour under these loadings. After that, an extensive parametric analysis is carried out to study the influencing mechanisms on the behaviour of the cable. Beneficial conclusions can be drawn as follows:

a). The axial strain-tension relationship is highly linear under tension as well as combined tension and external pressure. The wires bear the force chiefly.
b). The mechanical behaviour of the cable under torsion is linear before the slip occurs and the friction is found to be negligible. However, once slip occurs, the friction is indicated to influence the torsion stiffness of the cable significantly.
c). The wires bear tension when they are wound in the same direction as the torque, whereas the wires bear compression when they are wound in the opposite direction under torsion.
d). The increase of the water depth enlarges the wire stress and reduce the ability to resist axial tension. In ultra-deepwater areas, pressure armours might provide some help.
e). The less the winding angle is, the more the tension stiffness is. Nevertheless, the torsion stiffness does not have the same trend. The engineers can adjust the winding angle based on the decision of which stiffness is more important.

The proposed analytical model and its reliable results can not only provide references for the factory engineers during initial design and estimation, but also provide guidance for further investigation into other more complicated submarine power cables.

CRediT authorship contribution statement

Pan Fang: Conception and design of study, Funding acquisition, Formal analysis, Writing – original draft, revising the manuscript critically for important intellectual content. **Xiaoli Jiang:** Conception and

design of study, revising the manuscript critically for important intellectual content.

Declaration of competing interest

The authors declare the following financial interests/personal relationships which may be considered as potential competing interests:

Acknowledgment

The work was supported by the China Scholarship Council [grant number 201906320047]

References

Abaqus, V., 2014. 6.14 documentation, 651. Dassault Systemes Simulia Corporation, 6.2.
Bai, Y., Lu, Y., Cheng, P., 2015. Theoretical and finite-element study of mechanical behaviour of central, large-diameter umbilical cables under tension and torsion. Ships Offshore Struct. 10 (4), 393–403.
Bai, Y., et al., 2016a. Buckling stability of steel strip reinforced thermoplastic pipe subjected to external pressure. Compos. Struct. 152, 528–537.
Bai, Y., et al., 2016b. Analysis of steel strip reinforced thermoplastic pipe under internal pressure. Ships Offshore Struct. 11 (7), 766–773.
Bai, Y., et al., 2017. Mechanical behavior of metallic strip flexible pipe subjected to tension. Compos. Struct. 170, 1–10.
Bathe, K.-J., Bathe, Klaus-Jurgen, 2006. Finite element procedures.
Chang, H.-C., Chen, B.-F., 2019. Mechanical behavior of submarine cable under coupled tension, torsion and compressive loads. Ocean. Eng. 189, 106272.
Cornacchia, F., et al., 2019. Tensile strength of the unbonded flexible pipes. Compos. Struct. 218, 142–151.
Costello, G.A., Phillips, J.W., 1974. A more exact theory for twisted wire cables. J. Eng. Mech. Div. 100 (5), 1096–1099.
Costello, G.A., Phillips, J.W., 1975. Effective modulus of twisted wire cables. Department of Theoretical and Applied Mechanics, University of Illinois at ….
Dong, L., Zhang, Q., Huang, Y., 2013. Energy approaches based axisymmetric analysis of unbonded flexible risers, 41 (5). Huazhong Keji Daxue Xuebao(Ziran Kexue Ban)/ Journal of Huazhong University of Science and Technology(Nature Science Edition).
Fang, P., et al., 2018. Investigation on mechanical properties of fibreglass reinforced flexible pipes under torsion. Int. Conf. Offshore Mech. Arctic Eng. American Society of Mechanical Engineers.
Fang, P., et al., 2019. Mechanical responses of metallic strip flexible pipes subjected to pure torsion. Appl. Ocean Res. 86, 13–27.
Feret, J., Bournazel, C., 1987. Calculation of stresses and slip in structural layers of unbonded flexible pipes.
Gao, Y., et al., 2019. Investigation on mechanical properties of fiberglass reinforced flexible pipes under bending. Int. Conf. Offshore Mech. Arctic Eng. American Society of Mechanical Engineers.
Guo, Y., et al., 2017. Mechanical behavior analysis for unbonded umbilical under axial loads [J]. J. Ship Mech. 1007–7294.
Knapp, R., 1975. Nonlinear analysis of a helically armored cable with nonuniform mechanical properties in tension and torsion. OCEAN 75 Conference. IEEE.
Knapp, R., 1979. Derivation of a new stiffness matrix for helically armoured cables considering tension and torsion. Int. J. Numer. Methods Eng. 14 (4), 515–529.
Knapp, R., Shimabukuro, T.S., 2007. Structural analysis of composite umbilical cables. The Seventeenth International Offshore and Polar Engineering Conference. International Society of Offshore and Polar Engineers.
Longva, V., Sævik, S., 2016. On prediction of torque in flexible pipe reeling operations using a Lagrangian–Eulerian FE framework. Mar. Struct. 46, 229–254.
Love, A.E.H., 2013. A treatise on the mathematical theory of elasticity. Cambridge university press.
Merino, H.c.E., et al., 2009. On the coupled extensional–torsional response of flexible pipes. Int. Conf. Offshore Mech. Arctic Eng.
Panza, L., 2020. Mechanical performance study OF submarine power cables. Politecnico di Torino.
Ramos Jr., R., Kawano, A., 2015. Local structural analysis of flexible pipes subjected to traction, torsion and pressure loads. Mar. Struct. 42, 95–114.
Sævik, S., 2010. Comparison between theoretical and experimental flexible pipe bending stresses. Int. Conf. Offshore Mech. Arctic Eng.
Sævik, S., Ekeberg, K.I., 2002. Non-linear stress analysis of complex umbilical cross-sections. ASME 2002 21st international conference on offshore mechanics and arctic engineering. American Society of Mechanical Engineers Digital Collection.
Sævik, S., Gjøsteen, J., 2012. Strength analysis modelling of flexible umbilical members for marine structures. J. Appl. Math. 2012.
Skeie, G., Sødahl, N., Steinkjer, O., 2012. Efficient fatigue analysis of helix elements in umbilicals and flexible risers: theory and applications. J. Appl. Math. 2012.
Sun, X., et al., 2019. Analysis of polyester reinforced flexible composite pipe under internal pressure. Int. Conf. Offshore Mech. Arctic Eng. American Society of Mechanical Engineers.
Utting, W., Jones, N., 1987. The response of wire rope strands to axial tensile loads—Part II. Comparison of experimental results and theoretical predictions. Int. J. Mech. Sci. 29 (9), 621–636.
Witz, J., Tan, Z., 1992. On the axial-torsional structural behaviour of flexible pipes, umbilicals and marine cables. Mar. Struct. 5 (2–3), 205–227.
Xu, Y., et al., 2019. Structural analysis of fibreglass reinforced bonded flexible pipe subjected to tension. Ships Offshore Struct. 14 (7), 777–787.